

Effects of Interactions Between Filter Parasitics and Power Interconnects on EMI Filter Performance

Shuo Wang, *Senior Member, IEEE*, Jacobus Daniel van Wyk, *Fellow, IEEE*, and Fred C. Lee, *Fellow, IEEE*

Abstract—This paper first analyzes the electrical parameters of differential-mode (DM) and common-mode (CM) propagation on power interconnects. The impedance-transformation effects of the power interconnects are then investigated. The interactions between the parasitic parameters in electromagnetic-interference (EMI) filters and the transformed impedances by the power interconnects are explored in detail. It is found that the interactions can degrade EMI-filter performance at high frequencies. Simulations and experiments are finally carried out to verify the analysis.

Index Terms—Electromagnetic-interference (EMI) filter, equivalent parallel capacitance (EPC), equivalent series inductance (ESL), impedance transformation, power interconnects, transmission line.

I. INTRODUCTION

A TYPICAL conducted EMI-measurement setup for a power converter is shown in Fig. 1. Common-mode (CM) noise first flows through the parasitic capacitors between the converter and the ground plane. Most of the CM noise is then bypassed by the EMI filter through the ground point of the CM filter. At last, the remaining CM noise flows through the ground plane, the line impedance stabilization networks (LISNs), the power interconnects, and back to the EMI filter and the converter. In order to efficiently bypass CM noise, the grounding impedance of the CM filter should be as small as possible. On the other hand, the differential-mode (DM) noise in Fig. 1 is first attenuated by the DM filter and then flows between two power interconnects through LISNs. The noise is measured from the voltage drops of the noise current on the 50- Ω input impedances of the noise separator. In EMI measurements, it is sometimes found that there are unexpected noise peaks in the high-frequency (HF) range. For different cases, these noise peaks can be attributed to different mechanisms, such as the resonance of the ground loop [1]. This paper tries to analyze one of these mechanisms in relation to the measurement done including realistic power-line interconnects as encountered in practical measurement setup.

For the EMI measurement in Fig. 1, it is assumed that the DM load (here, it is the input impedance of the noise separator) of the EMI filter is 100 Ω because DM noise flows through two

series 50- Ω terminations of LISNs. It is also assumed that the CM load (here, it is the input impedance of the noise separator) of the EMI filter is 25 Ω because CM noise flows through the two parallel 50- Ω terminations of LISNs. This assumption holds when the distance between the equipment under test [a power-factor-correction (PFC) converter and an EMI filter] and the LISNs is short enough (for example, $< \lambda/20$) compared to the wavelength of measured EMI noise.

In a practical EMI-measurement setup for power electronic circuits, the length of the power interconnects between the EMI filter and the LISNs can be as long as 1–2 m or even more depending on the different applications. This makes the above assumption invalid because the transmission-line effects of the power interconnects make the load of the EMI filter no longer real 100 Ω for DM and real 25 Ω for CM. They may be capacitive or inductive, and their magnitude can also be much higher or lower than 100 and 25 Ω . These capacitive and inductive loads can interact with EMI filter's parasitics so as to worsen EMI-filter performance above 10 MHz. The phenomenon is attributed to the impedance transformation of the power interconnects. Since the HF noise can be very difficult to handle, it is important to investigate the mechanism of this interaction.

The recent publication [2] investigated the impedance compatibility between noise source, hybrid filter, and the LISNs to improve the filter's performance with impedance mismatch rule. The paper did not consider the effects of the power interconnects on filter's performance. Papers [3] and [4] design EMI filters based on the modeling of a noise source or EMI test receiver without considering the effects of the power interconnects, too. Paper [5] discusses the characteristics of a transmission line and how to utilize quarter-wavelength transmission lines to suppress harmonics of inverters. Other research on the impedance interactions of the EMI filters focuses on the stability issues that resulted from the interactions between the EMI filter and the PFC or dc/dc converters [6], [12], [13]. Paper [7] builds a CM-noise propagation model for the power-line cable using transmission-line theory, while it did not analyze the interactions between the parasitics of the EMI filters and the input impedance of the power interconnects. Paper [8] analyzed the performance of the EMI filter with arbitrary load and source impedance, which is beneficial to the analysis of this paper.

II. IMPEDANCE TRANSFORMATION OF POWER INTERCONNECTS

The power interconnects above a ground plane can be considered a transmission-line structure, which conducts both the DM

Manuscript received May 15, 2006; revised July 23, 2007.

S. Wang and F. C. Lee are with the Center for Power Electronics Systems, Virginia Tech, Blacksburg, VA 24060 USA (e-mail: shwang6@vt.edu).

J. D. van Wyk is with the Center for Power Electronics Systems, Virginia Tech, Blacksburg, VA 24060 USA, and also with the Department of Electrical and Engineering, University of Johannesburg, Johannesburg 2006, South Africa.

Color versions of one or more of the figures in this paper are available online at <http://ieeexplore.ieee.org>.

Digital Object Identifier 10.1109/TIE.2007.906126

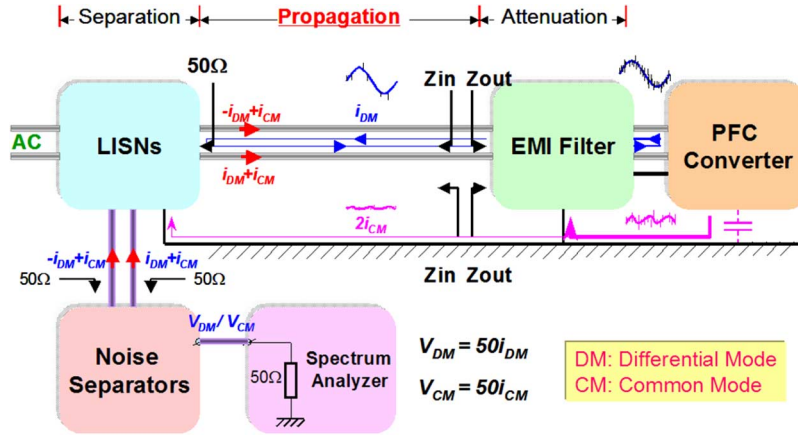


Fig. 1. Conducted EMI-measurement setup for a PFC converter.

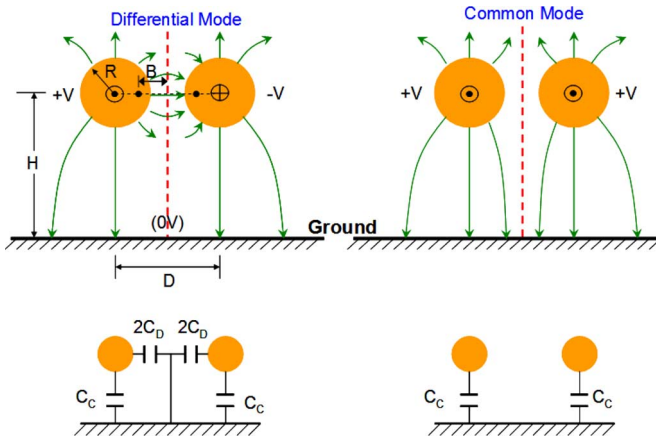


Fig. 2. Electrical parameters.

and CM noise. The impedance transformation can be analyzed using the transmission-line theory.

A. Electrical Parameters

The electrical parameters and the characteristic impedances for the DM and CM noise can be theoretically analyzed. Fig. 2 shows a cross-sectional view of round power interconnects and a ground plane. For the DM noise, voltages on the two interconnects have the same absolute value but with different polarities. For the CM noise, voltages on the two interconnects have the same absolute value and the same polarity. For convenience, it is assumed that the permittivity of the insulation layers is the same as that of air, that the two conductors perfectly conduct surface current, and that only TEM-mode waves propagate and no higher order mode waves are triggered. The static theory is therefore applied to electrical parameter calculation.

In Fig. 2, for the DM noise, due to the zero voltage potential of the center line, the capacitance between the power interconnects and the ground plane is composed of two parts, the capacitance C_C directly to the ground and the capacitance C_D between the power interconnects and the center line (zero voltage potential) [9]. For the CM noise, since no electrical flux crosses the center line, the capacitance C_D between the

two interconnects is zero, and then only the capacitance C_C between the ground and the power interconnects exists. Then the capacitances for the DM- and CM-noise propagation are given by [9]

$$C_{DM} = C_C + 2C_D \tag{1}$$

$$C_{CM} = C_C. \tag{2}$$

Using electromagnetic theory, it is not difficult to calculate the C_C and the C_D , and they are given in (3)–(5). The characteristic impedances are then given by (6)–(9). The c in equations is the speed of light. The approximation in (4) and (5) is held when H is much larger than R

$$B = \sqrt{(D/2)^2 - R^2} \tag{3}$$

$$C_C \approx 2\pi\epsilon_0 / \ln \left[\left(\frac{2H}{R} \right)^2 \frac{B - (D/2 - R)}{B + (D/2 - R)} \right] \tag{4}$$

$$C_D \approx \left[\frac{2\pi\epsilon_0 / \ln \left[\frac{2H}{R} \frac{B - (D/2 - R)}{B + (D/2 - R)} \right]}{\ln \left[\left(\frac{2H}{R} \right)^2 \frac{B - (D/2 - R)}{B + (D/2 - R)} \right] \cdot \ln \left[\frac{B + (D/2 - R)}{B - (D/2 - R)} \right]} \right], \tag{5}$$

DM between one power interconnect and the ground

$$Z_{0DM} = \sqrt{\frac{L_{DM}}{C_{DM}}} = \frac{1}{C_{DM} \cdot c}, \tag{6}$$

DM between two power interconnects

$$Z'_{0DM} = 2Z_{0DM}, \tag{7}$$

CM between one power interconnect and the ground

$$Z_{0CM} = \sqrt{\frac{L_{CM}}{C_{CM}}} = \frac{1}{C_{CM} \cdot c}, \tag{8}$$

and CM between two power interconnects and the ground

$$Z'_{0CM} = \frac{Z_{0CM}}{2}. \tag{9}$$

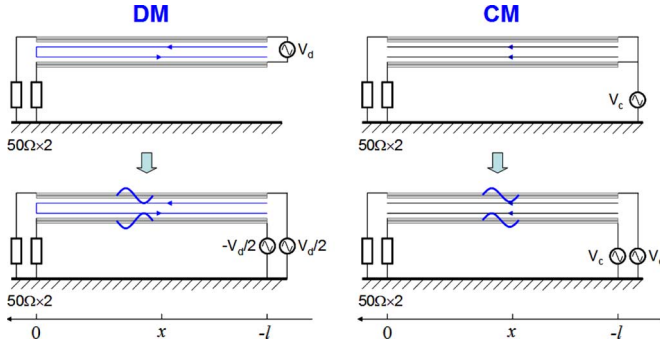


Fig. 3. Decoupling the noise propagation paths.

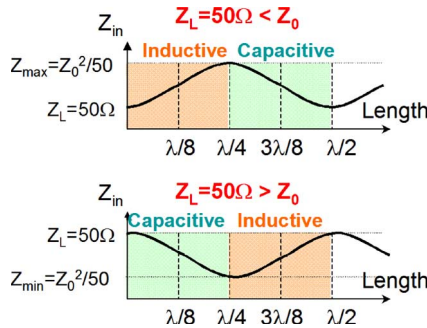


Fig. 4. Input impedance as a function of the length of power interconnects.

B. Impedance Transformation

It is assumed that the two power interconnects are perfectly balanced; thus, no transformation between the DM and CM noise happens. Both CM and DM propagation paths can be decoupled into two pairs of transmission lines, as shown in Fig. 3, where both CM and DM transmission lines are considered as the combination of one power interconnect and the ground plane. The characteristic impedances for the DM and CM transmission lines are therefore given by (6) and (8).

It is well known that the input impedance at any place x , along a transmission line, is described by (10), where $Z_{in}(x)$ is the input impedance at any place x on the power interconnects. Z_0 is the characteristic impedance of the transmission line; for the DM noise, it is Z_{0DM} , while for the CM noise, it is Z_{0CM} . λ is the wavelength of the noise. Z_L is load impedance; here, it is 50Ω .

$$Z_{in}(x) = Z_0 \frac{Z_L + jZ_0 \tan(2\pi/\lambda)x}{Z_0 + jZ_L \tan(2\pi/\lambda)x} \tag{10}$$

From (10), the input impedance at the source side ($x = -l$) depends on the noise frequency, the length of the power interconnects, and the load and characteristic impedance of the transmission line. The impedance transformation of the power interconnects can be easily analyzed using the Smith chart. The impedance as a function of the power-interconnect length is simply shown in Fig. 4.

In Fig. 4, when the characteristic impedance of the power interconnect is larger than the LISN’s input impedance of 50Ω , the magnitude of the input impedance of the power interconnect is always not smaller than 50Ω . In the first quarter-wavelength, the load of the EMI filter, i.e., the input impedance of the power

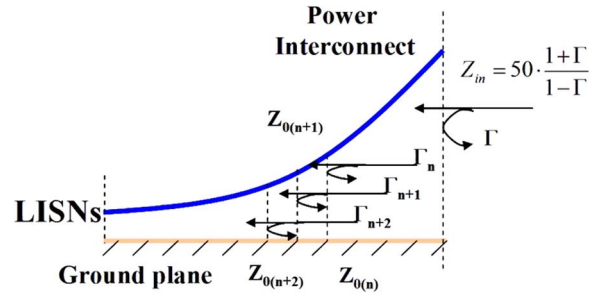


Fig. 5. Input impedance of nonhorizontal power interconnect can be characterized using reflection theory.

interconnects, is inductive. At quarter-wavelength, the maximal impedance is $Z_0^2/50$. In the second quarter-wavelength, the load of the EMI filter is capacitive. When the characteristic impedance of the power interconnect is smaller than the LISN’s input impedance of 50Ω , the magnitude of the input impedance of the power interconnect is always not larger than 50Ω . In the first quarter-wavelength, the load of the EMI filter, i.e., the input impedance of the power interconnects, is capacitive. At quarter-wavelength, the minimal impedance is $Z_0^2/50$. In the second quarter-wavelength, the load of the EMI filter is inductive. The quarter-wavelength at 30 MHz is 2.5 m. If the power interconnect between the EMI filter and the LISNs is not short enough and the characteristic impedance of the power interconnect is much different from 50Ω , the impedance transformation would be significant.

In a practical EMI-measurement setup, the power interconnects may not be parallel with the ground plane. In an extreme case, the power interconnects may even be perpendicular to the ground plane. For these cases, the characteristic impedance varies along the power interconnects. There will be wave reflections along the power interconnect due to the mismatch of the characteristic impedances. The total reflection coefficient Γ of the power interconnects can still be characterized using multireflection theory in [9], as shown in Fig. 5. The input impedance Z_{in} can therefore be calculated via (11). Z_{in} can also be inductive or capacitive depending on the characteristic impedances

$$Z_{in} = 50 \cdot \frac{1 + \Gamma}{1 - \Gamma} \tag{11}$$

III. INTERACTION WITH EMI FILTERS

EMI filters have output impedances, which are determined by the parasitic parameters in the EMI filters at HFs. A typical DM EMI filter and its model including parasitics are shown in Fig. 6 [8]. Because the impedances of the DM inductors are much higher than the impedance of C_2 , the output impedance of the DM EMI filter is determined by the output trace-loop impedance and the impedances of C_2 . The measured output impedance is shown in Fig. 7. A typical CM filter and its model are shown in Fig. 8. Because the impedances of the CM capacitors are much lower than the impedances of the CM inductors, as shown by the parasitic model in Fig. 8, the output impedance is determined by the CM inductors. The measured output impedance is shown in Fig. 9.

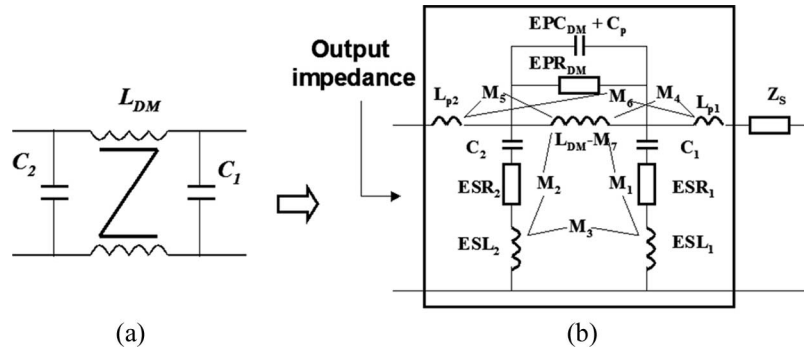


Fig. 6. DM EMI filter: (a) Circuit and (b) parasitic model.

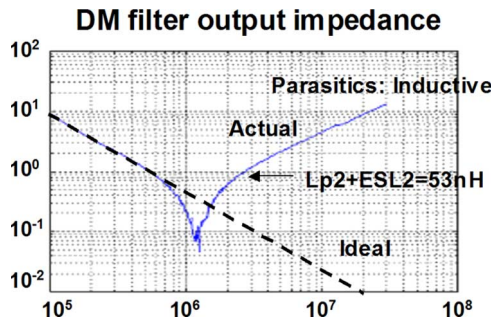


Fig. 7. Measured output impedance of the DM filter.

From Figs. 6–9, in the HF range, for the investigated EMI filter, the output impedance Z_{out} of the DM filter is determined by ESL_2 of the DM capacitor C_2 and the trace inductance L_{p2} . For the CM filter, Z_{out} is determined by the winding capacitance (EPC_{CM}) of the CM inductors. Since the DM and CM input impedances of the power interconnects are the loads of the EMI filter, they can interact with the output impedances of the DM and CM filters, respectively. The system being considered is shown in Fig. 10.

Table I illustrates the possible interaction between the EMI filter and the power interconnects. From Table I, the output impedances can resonate with the input impedances of the power interconnects. The resonances can cause noise voltage peaks on the real part of the input impedances. These noise peaks finally propagate to the LISN side with low attenuation because the power interconnects are assumed with low loss.

IV. EFFECTS ON EMI-FILTER PERFORMANCE

The interaction between the output impedances of the EMI filters and the input impedances of the power interconnects impacts the EMI-filter performance. The effects can be analyzed in Matlab. The S -parameters of EMI filters are first measured, and then it is transformed to T -parameters. The T -parameters of the EMI filter, together with the T -parameters of an ideal transmission line, are then used for cascade calculation. The final T -parameters are then transformed back to the S -parameters.

The calculations are carried out for four cases in Figs. 11–18. In Figs. 11 and 12, for the DM filter shown in Figs. 6 and 7, two cases are considered. For the first case, the characteristic impedance of the power interconnect is 5Ω , which is much

smaller than the LISN’s impedance of 50Ω . The small characteristic impedance could occur in some cases, for example, a power bus bar, which has a large capacitance and a small inductance between the two bars. For the second case, the characteristic impedance of the power interconnect is 500Ω , which is much larger than the LISN’s impedance of 50Ω . The large characteristic impedance could happen when the distance between the two power interconnects is much larger than the conductor’s dimensions, which has a large inductance and a small capacitance between the two power interconnects. For both cases, the noise-source impedance used for calculation is a $300\text{-}\mu\text{H}$ PFC inductor.

In Fig. 11, when Z_0 is 5Ω , the input impedance of the power interconnects is capacitive if the length of the power interconnects between the LISNs and the EMI filter is smaller than a quarter-wavelength of noise frequency. An $R(f) - C(f)$ equivalent circuit is derived for the power interconnects. Because the output impedance of the investigated DM EMI filter is inductive at HFs, series resonance could happen at HFs. The resonant frequency varies with the length of the power interconnects. The longer the power interconnects, the lower the series resonant frequency. For the case in Fig. 12 when Z_0 is 500Ω , an $R(f) - L(f)$ equivalent circuit is derived for the power interconnects. If the noise frequency is higher than the corner frequency $R(f)/(2\pi(L(f) + ESL + L_{p2}))$, the noise is attenuated. The calculated 3-D (power-interconnect length–noise frequency–noise ratio in decibels: amplitude on LISNs with power interconnect to that without power interconnects) results are shown in Figs. 13 and 14 for 5- and $500\text{-}\Omega$ characteristic impedances, respectively.

In Fig. 13, the peak shows up at 30 MHz when the interconnect length is 1 m . It moves down to 18 MHz when interconnect length increases to 2.5 m . Compared to the case without the power interconnects, the noise is amplified by $10\text{--}17 \text{ dB}$ when the peak shows up. This verifies the previous analysis. Since longer power interconnect causes larger input capacitance, resonant frequency will become lower. In Fig. 14, the EMI-filter performance is significantly improved at 30 MHz when the power-interconnect length is 1 m . The improvement point moves down to 18 MHz when the length increases to 2.5 m . Compared to the case without the power interconnects, the noise is reduced by up to 17 dB at HFs since the frequency of the HF noise becomes higher than the corner frequency of the equivalent circuit. This verifies the previous analysis. Longer

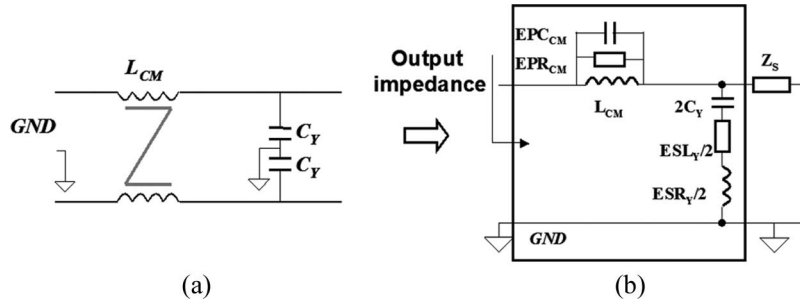


Fig. 8. CM EMI filter: (a) Circuit and (b) parasitic model.

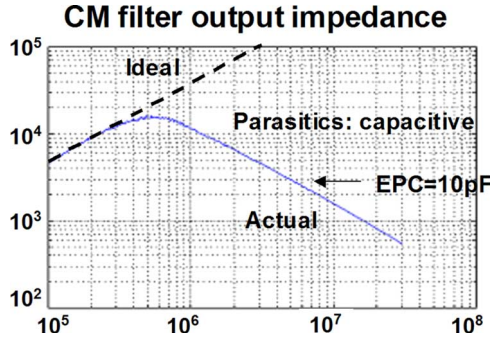


Fig. 9. Measured output impedance of the CM filter.

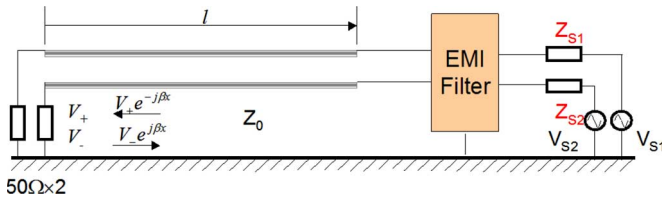


Fig. 10. EMI filter with noise source, power interconnects, and load.

power interconnects cause larger input inductance, so the corner frequency of the equivalent circuit in Fig. 12 becomes lower. As a result, the noise is attenuated to lower levels at HF.

In Figs. 15 and 16, for the CM filter shown in Figs. 8 and 9, two cases are considered. For the first case, the characteristic impedance of the power interconnects is 5 Ω, which is much smaller than the LISN’s impedance of 50 Ω. This small characteristic impedance could occur when a power bus-bar pair is located very close to the ground plane, which has a large capacitance and a small inductance. For the second case in Fig. 16, the characteristic impedance of the power interconnects is 500 Ω, which is much larger than the LISN’s impedance of 50 Ω. This large characteristic impedance could occur when the distance between the two power interconnects and the ground plane is much larger than the power-interconnect conductor’s dimensions, which has a large inductance and a small capacitance. For both cases, a 100-pF capacitor is used to represent the noise-source impedances of the CM noise. The calculated 3-D (power-interconnect length–noise frequency–noise ratio in decibels: amplitude on LISNs with power interconnect to that without power interconnects) results are shown in Figs. 17 and 18 for 5- and 500-Ω characteristic impedances, respectively. In Fig. 15, an $R(f) - C(f)$ equivalent circuit is derived for the power interconnects. If the frequency of noise is lower

than the corner frequency of $(C(f) + EPC_{CM}) / (2\pi R(f) \times EPC_{CM} \times C(f))$, the noise is attenuated. In Fig. 16, an $R(f) - L(f)$ equivalent circuit is derived for the power interconnects because the characteristic impedance is higher than 50 Ω. There is a resonance in the output loop of the CM filter since the output impedance is the winding capacitance EPC_{CM} .

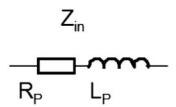
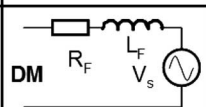
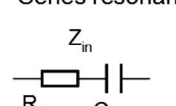
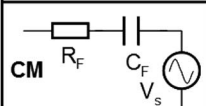
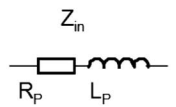
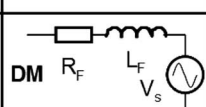
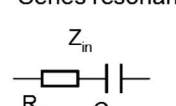
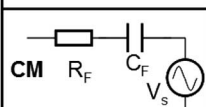
In Fig. 17, the filter performance at HF is better than the case without the power interconnects since the frequency of the HF noise becomes lower than the corner frequency of the equivalent circuit. In Fig. 18, the peak shows up at 30 MHz when the interconnect length is 1 m. It moves down to 18 MHz when the interconnect length increases to 2.5 m since a longer interconnect causes larger input inductance. Compared to the case without the power interconnect, the noise is amplified by 6–14 dB when the peak shows up. This verifies the previous analysis.

Based on these calculations and analysis, it is found that the DM-filter performance can be worse at HF due to the interactions between the power interconnects and the filter trace inductance plus the equivalent series inductance (ESL) of the DM capacitor in the filter. CM-filter performance can be worse at HF due to the interactions between the power interconnects and the winding capacitance of the CM inductors in the filter.

In order to prevent adverse interaction, the output-loop inductances of the DM filter and the ESL of the DM capacitor should be as small as possible. The winding capacitance of the CM inductor should be as small as possible. The measurement setup is also an important contributor to the filter performance at HF. If the characteristic impedance is near load impedance, noise-peak values would be much lower. If the length of the power interconnects between the EMI filter and the LISNs is short, for example, shorter than 0.5 m, the possibilities for noise peaks would be much lower. As stated at the end of Section II, in a practical EMI-measurement setup, the distance between the power interconnects and the ground plane is not constant; thus, the characteristic impedance varies along the power interconnects. As a result, the magnitude of reflection coefficients also varies along the power interconnects. The reflection coefficients at the EMI-filter side can still be estimated by characterizing the power interconnects and the LISNs as a network, as shown in Fig. 19.

In Fig. 19, the power interconnect–LISN network is characterized by a DM $S[S]_{DM}^a$ matrix and a CM $S[S]_{CM}^a$ matrix. The effects of parasitics of the LISNs and ground wires are included in the S matrices. The impedance-transformation effects of the power interconnects and the LISNs can then be

TABLE I
INTERACTION BETWEEN THE FILTER AND THE POWER INTERCONNECTS ($l < \lambda/4$)

Z _{in} (Power Interconnects)	EMI Filter (HF)	Possible Effects
$Z_0 > Z_L$  Series resonance	 DM	Noise level depends on time constant
$Z_0 < Z_L$  Series resonance	 CM	High noise level created at resonant frequency
$Z_0 > Z_L$  Series resonance	 DM	High noise level created at resonant frequency
$Z_0 < Z_L$  Series resonance	 CM	Noise level depends on time constant

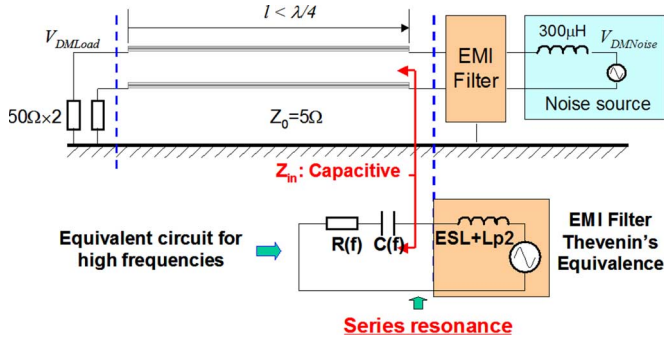


Fig. 11. Effects of power interconnects on DM EMI-filter performance: $Z_0 < 50 \Omega$.

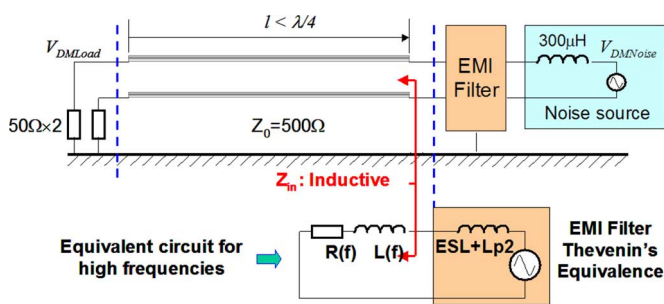


Fig. 12. Effects of power interconnects on DM EMI-filter performance: $Z_0 > 50 \Omega$.

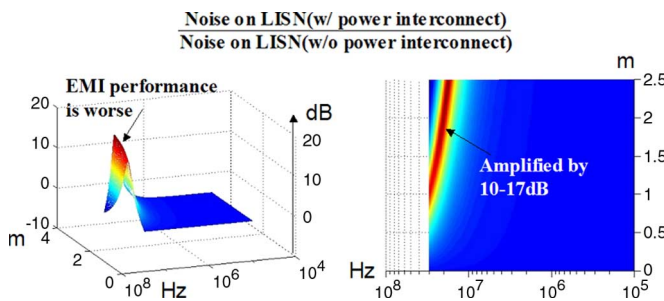


Fig. 13. DM-noise analysis when $Z_0 = 5 \Omega$.

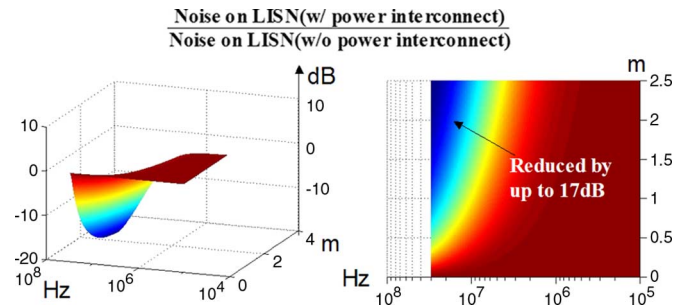


Fig. 14. DM-noise analysis when $Z_0 = 500 \Omega$.

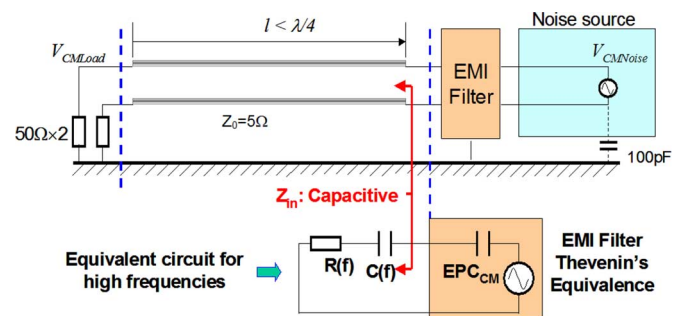


Fig. 15. Effects of power interconnects on CM EMI-filter performance: $Z_0 < 50 \Omega$.

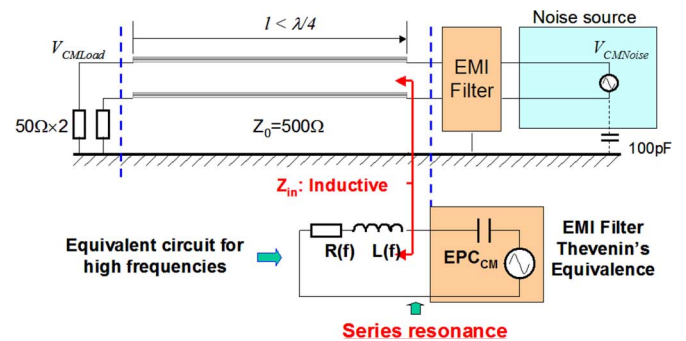


Fig. 16. Effects of power interconnects on CM EMI-filter performance: $Z_0 > 50 \Omega$.

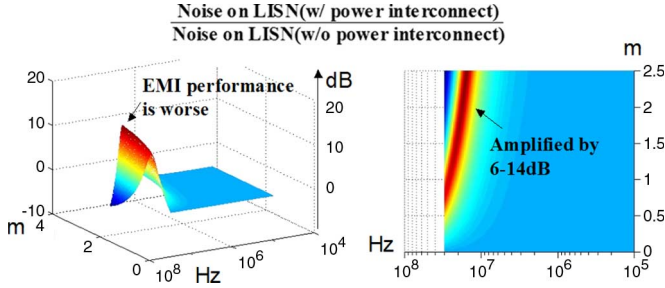


Fig. 17. CM-noise analysis when $Z_0 = 5 \Omega$.

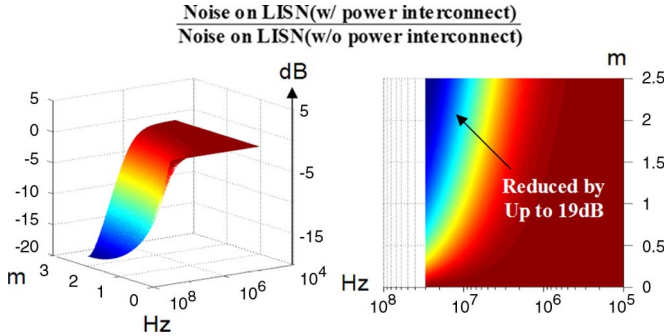


Fig. 18. CM-noise analysis when $Z_0 = 500 \Omega$.

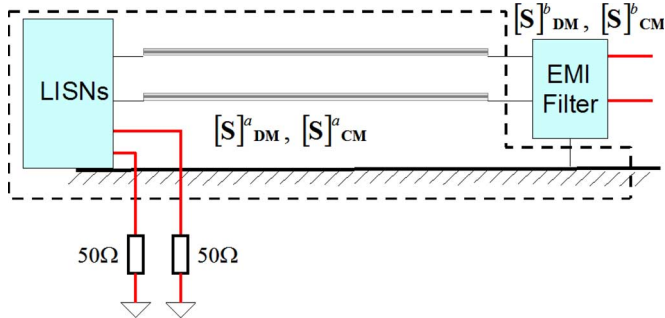


Fig. 19. Characterizing the power interconnects and the LISNs as a network.

analyzed from the DM reflection coefficients Γ_{DM} and the CM reflection coefficients Γ_{CM} . Γ_{DM} and Γ_{CM} are first calculated from the measured $[S]_{DM}^a$ and $[S]_{CM}^a$ matrices. The interaction between the input impedances Z_{inDM} and Z_{inCM} of the power interconnect–LISN network and the output impedances of the DM and CM filters can then be analyzed.

V. EXPERIMENTS

The experiments were carried out in an EMI chamber, and the setup is shown in Fig. 20. One power cable, which is used as an interconnect, is laid out randomly in the experiment. The distance between the LISNs and the EMI filter is 1.2 m. An Agilent four-port ENA RF network analyzer E5070B [10] is used in the experiment. In the experiment, $[S]_{DM}^a$ and $[S]_{CM}^a$ of the power interconnect–LISN network are first measured. The input impedances are then calculated. Second, the $[S]_{DM}^b$ and $[S]_{CM}^b$ of the EMI filter are measured, and the output impedances are calculated. By analyzing these input and output impedances, the possible resonant frequencies are identified. At last, the DM and CM S matrices of the whole system

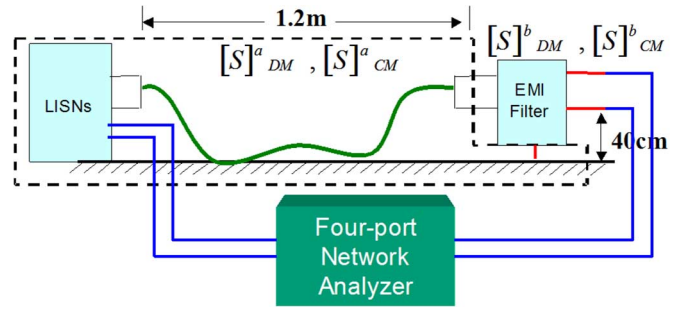


Fig. 20. Experiment setup: Power cable is laid out randomly.

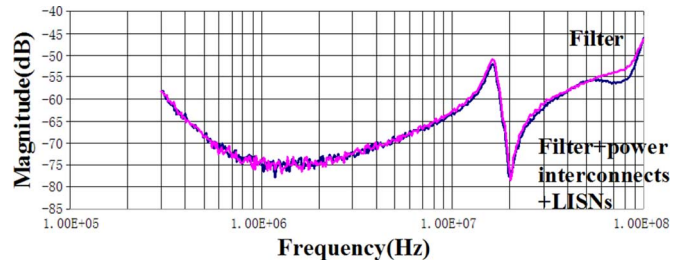


Fig. 21. Comparison of SDD21 on DM propagation.

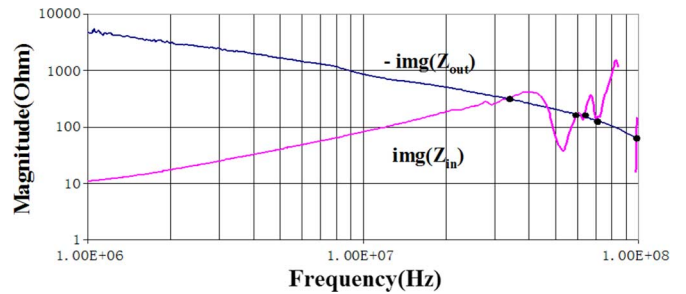


Fig. 22. Imaginary parts of the input and output impedances.

(EMI filter–power interconnects–LISNs) are measured. The measured results are explained by the results from the first two experiments.

For the DM part, the transmission-line effects are not significant. The measured reflection coefficient is actually smaller than -20 dB up to 50 MHz. The measured characteristic impedance of the power cable is around 103Ω , which is very close to the $100\text{-}\Omega$ DM load impedance. For the power cable, two conductors are very close to each other; therefore, the C_D is much larger than the C_C . The effects of the ground plane on the DM characteristic impedance are insignificant. SDD21 of the EMI filter–power interconnects–LISNs is almost the same as the EMI filter, as shown in Fig. 21. The peak and dip around 20 MHz on both curves are due to the resonances between the CM and DM capacitors in the EMI filter [11]. For the CM part, the distance between the power interconnects and the ground plane plays a role since the C_C determines the CM characteristic impedance. The imaginary part of the input impedance of the power interconnects–LISNs and the imaginary part of the output impedance of the CM EMI filter are calculated from the measured CM S matrices and are compared in Fig. 22. The resonance occurs when the imaginary parts cancel each other. Fig. 23 shows the comparison of the measured SCC21

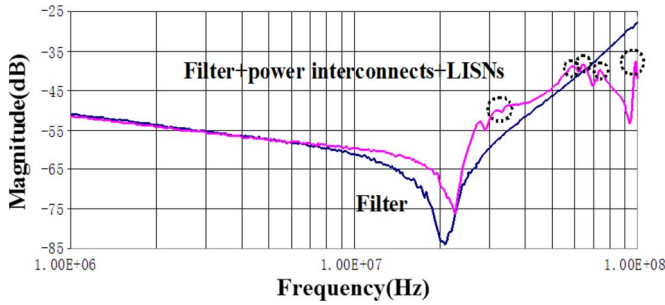


Fig. 23. Comparison of SCC21 on CM propagation.

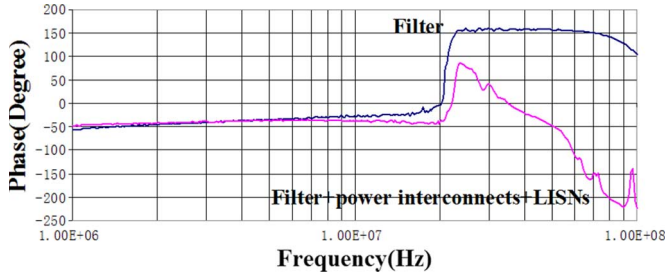


Fig. 24. Phases of SCC21.

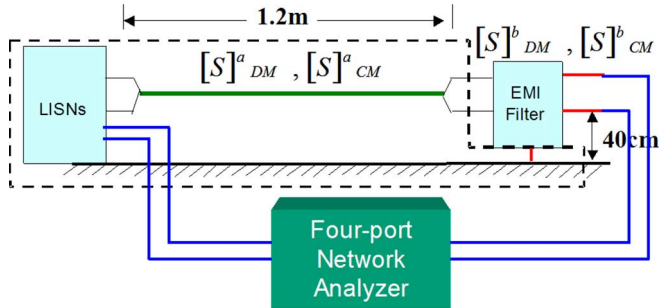


Fig. 25. Experiment setup: Power interconnects are more above ground plane.

between the filter and the whole system (EMI filter–power interconnects–LISNs).

In Fig. 22, the output impedance of the filter is the winding capacitance of the CM inductor. The input impedance of the power interconnects is inductive below 40 MHz since the characteristic impedance of the power interconnects is larger than the load impedance. At frequencies above 40 MHz, the input impedance is somewhat complicated because of the varying characteristic impedance along the interconnects and the mismatched load at the ends of the interconnects. The imaginary curve of the input impedance is not shown from 83 to 97 MHz in Fig. 22 since it is negative in that frequency range. From Fig. 22, the two curves cross at 34, 48, 59, 63, 71, and 98 MHz. The imaginary parts cancelled each other at these frequencies. Based on previous analysis, series resonances would happen at these frequencies, and peaks would show up on the SCC21 curve. In Fig. 23, at corresponding frequencies, peaks show up on the curve of filter–power interconnects–LISNs, which proves the interaction between the parasitics of the EMI filters and the impedance transformed by the power interconnects. The 48-MHz cross point in Fig. 22 does not cause a peak in Fig. 23 because of the capacitive behavior of input impedance at that frequency. Fig. 24 shows the corresponding phases of

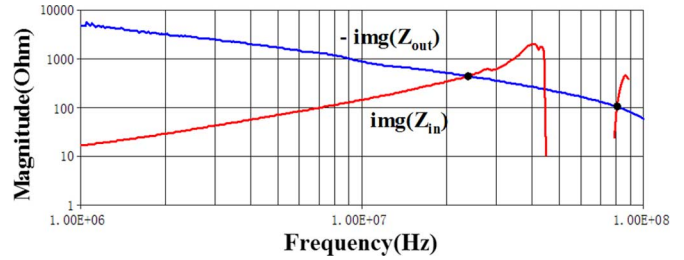


Fig. 26. Imaginary parts of input and output impedances.

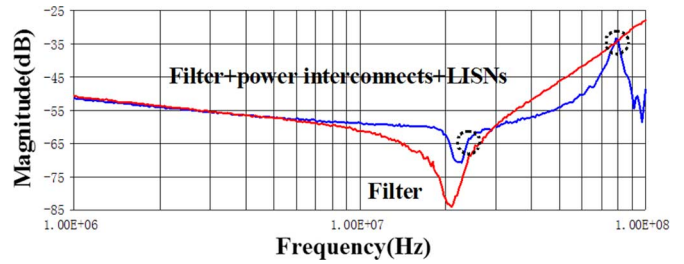


Fig. 27. Comparison of SCC21 on CM propagation.

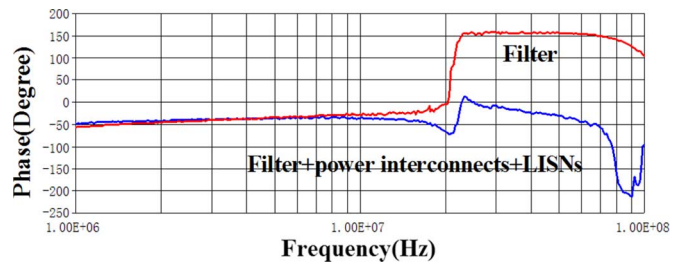


Fig. 28. Phases of SCC21.

SCC21. Comparing the two curves in Fig. 23, the resonance at 34 MHz degrades the filter performance by up to 13 dB from 8 to 30 MHz. The actual filter performance is kept degraded until 65 MHz due to other resonances. The interaction between the winding capacitance of the CM inductors in the filter and the impedance transformed by the power interconnects could therefore be an important issue for HF analysis. The second experiment is carried out by increasing the distance between the power interconnects (power cable) and the ground plane. The setup is shown in Fig. 25. From (2), (4) and (8), it is expected that the CM characteristic impedance is higher than the previous case. As a result, the CM input impedance would be more inductive than the previous case. The first resonance frequency should be lower than that in the first experiment. Figs. 26–28 show the results.

In Figs. 26 and 27, the first resonance shows up at 24 MHz, which is very close to the series resonant frequency (21 MHz) of the CM capacitors (due to ESL_Y). As a result, the two resonances partly cancel each other. This is clearly shown on the phase curves in Fig. 28. The cross point around 80 MHz in Fig. 26 causes a resonance on the SCC21 curve in Fig. 27. The imaginary curve of the input impedance is not shown in Fig. 26 from 45 to 79 MHz since it is negative in that frequency range (input impedance is capacitive in the second quarter-wavelength). The performance of the filter is degraded by up to 20 dB in the frequency range of 6–30 MHz due to the resonance

between the winding capacitance of the CM inductors in the filter and the impedance transformed by the power interconnects. It should be pointed out that if the length of the power interconnects is longer than that in the experiments, which may happen in many power electronic applications, the resonant frequency would be at lower frequencies so that the filter's low-frequency performance will be degraded.

VI. CONCLUSION

This paper first analyzed the electrical parameters for both the DM and CM propagation on power interconnects. Power interconnects are then considered as transmission lines with an impedance-transformation function. As a result, the input impedances of power interconnects, i.e., the loads of the DM and CM EMI filters, are no longer the LISN's real 50- Ω impedances but are the capacitive or inductive impedances. These impedances can interact with the parasitic parameters of the EMI filters and degrade the filters' performance at HFs. Finally, both simulations and experiments are carried out to prove the analysis. Solutions are proposed to avoid these interactions.

REFERENCES

- [1] S. Wang, F. C. Lee, D. Y. Chen, and W. G. Odendaal, "Effects of parasitic parameters on the performance of EMI filters," in *Proc. IEEE Power Electron. Spec. Conf.*, Acapulco, Mexico, Jun. 15–19, 2003, pp. 73–78.
- [2] W. Chen, X. Yang, and Z. Wang, "Analysis of insertion loss and impedance compatibility of hybrid EMI filter based on equivalent circuit model," *IEEE Trans. Ind. Electron.*, vol. 54, no. 4, pp. 2057–2120, Aug. 2007.
- [3] J. Meng, W. Ma, Q. Pan, Z. Zhao, and L. Zhang, "Noise source lumped circuit modeling and identification for power converters," *IEEE Trans. Ind. Electron.*, vol. 53, no. 6, pp. 1853–1861, Dec. 2006.
- [4] T. Nussbaumer, M. L. Heldwein, and J. W. Kolar, "Differential mode input filter design for a three-phase buck-type PWM rectifier based on modeling of the EMC test receiver," *IEEE Trans. Ind. Electron.*, vol. 53, no. 5, pp. 1649–1661, Oct. 2006.
- [5] T. Shimizu and M. Shioya, "Characteristics of electric power transmission on high-frequency inverter having distributed constant line at load side," *IEEE Trans. Ind. Electron.*, vol. 38, no. 2, pp. 115–120, Apr. 1991.
- [6] G. Spiazzi and J. A. Pomilio, "Interaction between EMI filter and power factor preregulators with average current control: Analysis and design considerations," *IEEE Trans. Ind. Electron.*, vol. 46, no. 3, pp. 577–584, Jun. 1999.
- [7] K. Y. See, P. L. So, A. Kamarul, and E. Gunawan, "Radio-frequency common-mode noise propagation model for power-line cable," *IEEE Trans. Power Del.*, vol. 20, no. 4, pp. 2443–2449, Oct. 2005.
- [8] S. Wang, F. C. Lee, and W. G. Odendaal, "Characterization and parasitic extraction of EMI filters using scattering parameters," *IEEE Trans. Power Electron.*, vol. 20, no. 2, pp. 502–510, Mar. 2005.
- [9] R. E. Collin, *Foundations for Microwave Engineering*, 2nd ed. New York: McGraw-Hill, 1992.
- [10] *Agilent E5070B/E5071B ENA Series RF Network Analyzers User's Guide*, Agilent Technol., Palo Alto, CA, 2004.
- [11] S. Wang, J. D. van Wyk, F. C. Lee, and W. G. Odendaal, "Transformation between common mode and differential mode due to the imperfect balance of EMI filters," in *Proc. CPES Power Electron. Conf.*, Blacksburg, VA, Apr. 17–20, 2005, pp. 551–555.
- [12] K. Louati, D. Sadarnac, and C. Karimi, "Input filter influence on the control stability of DC/DC converters," in *Proc. IEEE Int. Symp. Ind. Electron.*, May 4–7, 2004, vol. 2, pp. 1165–1171.
- [13] A. Altowati, T. Suntio, and K. Zenger, "Input filter interactions in multi-module parallel switching-mode power supplies," in *Proc. IEEE Int. Conf. Ind. Technol.*, Dec. 15–17, 2005, pp. 851–856.
- [14] B.-R. Lin and C.-H. Huang, "Implementation of a three phase capacitor clamped active power filter under unbalanced condition," *IEEE Trans. Ind. Electron.*, vol. 53, no. 5, pp. 1621–1630, Oct. 2006.
- [15] M. E. Ortúzar *et al.*, "Voltage-source active power filter based on multi-level converter and ultracapacitor DC link," *IEEE Trans. Ind. Electron.*, vol. 53, no. 2, pp. 477–485, Apr. 2006.



Shuo Wang (S'03–M'06–SM'07) received the B.S.E.E. degree from Southwest Jiaotong University, Chengdu, China, in 1994, the M.S.E.E. degree from Zhejiang University, Hangzhou, China, in 1997, and the Ph.D. degree from the Center for Power Electronics Systems (CPES), Virginia Polytechnic Institute and State University (Virginia Tech), Blacksburg, in 2005.

Since 2005, he has been a Research Assistant Professor with the CPES, Virginia Tech. From 1997 to 1999, he was with Zhong Xing Telecommunication Equipment Corporation, Shenzhen, China, where he was a Senior R&D Engineer and was responsible for the development and support of power supply for wireless products. In 2000, he worked with UTStarcom Telecom Company, Ltd., Hangzhou, where he was responsible for the development and support of optical access networks. He holds one U.S. patent and has three U.S. patents pending.

Dr. Wang received the 2005 Best Transaction Paper Award from the IEEE TRANSACTIONS ON POWER ELECTRONICS and the William M. Portnoy Award for the best paper published in IEEE IAS Annual Conference in 2004. He is an Associate Editor for the IEEE TRANSACTIONS ON INDUSTRY APPLICATIONS.



Jacobus Daniel van Wyk (F'90) received the M.Sc.Eng. degree from the University of Pretoria, Pretoria, South Africa in 1966, the Dr.Sc.Tech. degree (*cum laude*) from the Technical University, Eindhoven, Netherlands, in 1969, and the D.Sc. (Eng.) degree (*honoris causa*) from the University of Natal, Durban, South Africa, in 1996.

He is currently with both the Center for Power Electronics Systems, Virginia Tech, Blacksburg, and the Department of Electrical and Electronic Engineering Science, University of Johannesburg, Johannesburg, South Africa. He has worked and published in the fields of semiconductors, microelectronics, electric materials, electromechanical energy conversion, electric drives, power electronics, industrial electronics, control, alternative energy systems, electric vehicles, and many diverse applications in industry, mining, transportation, and electrical-energy-supply systems. His present research interest is in integrated electronic power processors.

Dr. van Wyk is a Fellow of the South African Institute of Electrical Engineers. He has been a recipient and a corecipient of 20 prize paper awards including 11 IEEE prize paper awards for some of his works, and was the recipient of the prestigious IEEE William E. Newell Power Electronics Award in 1995 and the IEEE Third Millennium Medal in 2000. He has received a range of other awards from IEEE societies as well as from the South African Institute of Electrical Engineers. He was the Editor-in-Chief of the IEEE TRANSACTIONS ON POWER ELECTRONICS from 2002 to 2006.



Fred C. Lee (S'72–M'74–SM'87–F'90) received the B.S. degree in electrical engineering from National Cheng Kung University, Tainan, Taiwan, R.O.C., in 1968 and the M.S. and Ph.D. degrees in electrical engineering from Duke University, Durham, NC, in 1972 and 1974, respectively.

He is currently a University Distinguished Professor with Virginia Tech, Blacksburg. He directs the Center for Power Electronics Systems, a National Science Foundation engineering research center whose participants include five universities and over 80 corporations. He holds 30 U.S. patents and has published over 175 journal articles in refereed journals and more than 400 technical papers in conference proceedings.

Dr. Lee is a recipient of the Society of Automotive Engineering's Ralph R. Teeter Education Award (1985), Virginia Tech's Alumni Award for Research Excellence (1990), and Virginia Tech College of Engineering Dean's Award for Excellence in Research (1997). In 1989, he received the William E. Newell Power Electronics Award. He is also a recipient of the Arthur E. Fury Award for Leadership and Innovation in Advancing Power Electronic Systems Technology (1998) and the IEEE Millennium Medal.